Micromagnetic modeling of anisotropic damping in magnetic nanoelements

Mykola Dvornik,* Arne Vansteenkiste, and Bartel Van Waeyenberge
DyNaMat Lab, Ghent University, Krijgslaan 281/S1, 9000 Ghent, Belgium
(Received 9 May 2013; revised manuscript received 15 July 2013; published 29 August 2013)

We report a numerical implementation of the Landau-Lifshitz-Baryakhtar theory that dictates that the micromagnetic relaxation term obeys the symmetry of the magnetic crystal, i.e., replacing the single intrinsic damping constant with a tensor of corresponding symmetry. The effect of anisotropic relaxation is studied in a thin saturated ferromagnetic disk and an ellipse with and without uniaxial magnetocrystalline anisotropy. We investigate the angular dependence of the linewidth of magnonic resonances with respect to the given structure of the relaxation tensor. The simulations suggest that the anisotropy of the magnonic linewidth is determined by two factors: the projection of the relaxation tensor onto the plane of precession and the ellipticity of the latter.

DOI: 10.1103/PhysRevB.88.054427 PACS number(s): 75.30.Ds, 75.78.Cd, 75.75.Jn, 76.50.+g

Landau and Lifshitz[1] and later Gilbert[2,3] introduced a phenomenological relaxation term in the equation of motion of magnetic moments in ferromagnetic media. They suggested that the magnetic losses can be characterized by a single intrinsic damping constant of relativistic nature. Both the Landau-Lifshitz and the Gilbert phenomenological damping terms are essentially equivalent for low magnetic losses, while the Gilbert damping term works better for large values of the damping constant, as was pointed out by Kikuchi.[4] These terms are now widely used for the description of magnetic relaxations in magnetic thin films[5,6] and patterned magnetic media.[7] The microscopic mechanism behind the magnetic losses in metals has also been suggested, e.g., in Gilmore *et al.*[8]

However, recent experimental data urge the development of new micromagnetic approaches to the description of magnetic losses, i.e., by introducing higher-order terms within the Gilbert approach,[9] inert relaxation,[10] and by generalizing the magnetization dynamics and relaxation within the framework of Onsager's kinetic equations.[11] The latter approach shows that the relaxation part of the equation of precession should obey the crystallographic symmetry of the media, thereby replacing the single intrinsic damping constant with a tensor. The reason behind anisotropic relaxation in magnetic media is the symmetry of the spin-orbit and *s-d* interaction,[12] which couples the spins to the other subsystems (degrees of freedom), i.e., the lattice and the free electrons, respectively. It is worth noting that an angular dependence of magnetic losses (or effects associated with the same physics) has already been reported experimentally.[13–18] However, analytical and numerical approaches still have to be developed, especially for nanoscale structures where the magnetic resonances are strongly confined, and so, their spectra are discrete.

In this paper, we report on a numerical implementation of Baryakhtar's theory[11] within the mumax2 micromagnetic framework.[19] Furthermore, we systematically investigate the influence of anisotropic relaxation on the angular dependence of ferromagnetic resonance (FMR) linewidths in a nanoscale magnetic disk and an ellipse.

We start from the general Baryakhtar equation (LLBar),

$$\frac{\partial \mathbf{M}}{\partial t} = -\gamma_{\mathrm{LL}}\mathbf{M}\times\mathbf{H} + \hat{\lambda}(\mathbf{M})\mathbf{H} - \hat{\lambda}^{(e)}_{pq}(\mathbf{M})\frac{\partial^2\mathbf{H}}{\partial x_p \partial x_q}, \qquad (1)$$

where $\mathbf{M}$, γ_{LL}, $\mathbf{H}$ are the magnetization vector, the positively defined gyromagnetic ratio, and the effective internal field, respectively. The first term in the equation defines the torque, while the second and third describe the local and nonlocal[20] relaxations, respectively. $\hat{\lambda}(\mathbf{M})$ and $\hat{\lambda}^{(e)}(\mathbf{M})$ are the relaxation tensors of relativistic and exchange nature, respectively, and in general are functions of the magnetization vector. These tensors are in fact operators that describe how crystallographic and magnetic symmetries of the system contribute to the relaxation of magnons. It is worth noting that in contrast to the Landau-Lifshitz formalism, Baryakhtar's equation does not conserve the length of the magnetization vector, i.e., $|\mathbf{M}| \neq \text{const}$. This is especially the case for magnetic metals. So in contrast to the Landau-Lifshitz theory, Baryakhtar's equation can correctly describe the magnetic relaxations in metals.

In planar magnetic nanoelements the internal magnetic field is nonuniform, e.g., due to the magnetodipolar field. So according to Eq. (1) the static contribution of the nonlocal damping might reduce the magnetization vector length. Nevertheless, in the intermediate range of temperatures such relativistic effect cannot compete with the exchange force that tries to keep the magnetization vector length constant. So in contrast to Ref. 13, variations of the magnetization vector length are vanishing and cannot significantly contribute to the magnon-magnon scattering and, thereby, to the FMR linewidth broadening. On the other hand, the dynamic contribution of the nonlocal damping becomes significant only when the wavelength of magnons approaches the exchange length of the material,[21] i.e. for high-order exchange dominated spin waves. For the sake of simplicity, this paper focuses on the lowest-order magnetic resonances, i.e. magnetostatic magnons. So both static and dynamic contributions of the nonlocal damping are vanishing, i.e., $\hat{\lambda}^{(e)}_{pq}\frac{\partial^2\mathbf{H}}{\partial x_p \partial x_q} \ll \hat{\lambda}H$, and Eq. (1) reduces to

$$\frac{\partial \mathbf{M}}{\partial t} = -\gamma_{\mathrm{LL}}\mathbf{M}\times\mathbf{H} + \hat{\lambda}(\mathbf{M})\mathbf{H}. \qquad (2)$$

The exact form of the relativistic tensor $\hat{\lambda}(\mathbf{M})$ is unknown for an arbitrary magnetic configuration. However, the tensor can be expanded into combinations of the magnetization vector components that are invariant with respect to the magnetic symmetry of the system, i.e., $\hat{\lambda}(\mathbf{M}) = \hat{\lambda}(0) + \hat{\mu}_{pq}(0)M_pM_q + \cdots$, where $\hat{\lambda}(0)$ and $\hat{\mu}_{pq}(0)$ are zero- and second-order

relativistic relaxation tensors. The coefficients of the expansion take into account crystallographic symmetry, while the combinations of M represent symmetry invariants of the magnetic ground state. The expansion is taken in the vicinity of the absolutely symmetric state $M = 0$,[22,23] and p,q denote spatial components that do not mix with corresponding crystallographic indices of $\hat{\mu}$. According to Ref. 22, the first term in the expansion describes nonconservative relaxations, where energy dissipation is accompanied with angular momentum transfer. This mechanism dominates in ferromagnetic metals as became evident from experiments on ultrafast demagnetization.[24,25] Therefore we omit the higher-order terms in the Taylor expansion, so that $\hat{\lambda}(\mathbf{M}) \approx \hat{\lambda}(0) = -\gamma_{\mathrm{LL}} M_s \hat{\alpha}$, where $\hat{\alpha}$ is a dimensionless damping tensor and M_s denotes the length of magnetization vector at zero temperature. The approximation implies temperatures that are far away from the Curie point, where second-order effects start to play a role. So our numerical implementation is valid for the intermediate range of temperatures, where the majority of experiments are performed. So, finally Eq. (2) transforms into

$$\frac{\partial \mathbf{M}}{\partial \mathrm{t}} = -\gamma_{\mathrm{LL}} \mathbf{M} \times \mathbf{H} - \gamma_{\mathrm{LL}} M_s \hat{\alpha} \mathbf{H}, \tag{3}$$

which under assumption of constant magnetization length and isotropic relaxations, $\hat{\alpha} = \alpha \hat{I}$, where $\hat{I}$ is the unit tensor, transforms into the well-known Landau-Lifshitz equation (LL) $\frac{\partial \mathbf{M}}{\partial \mathrm{t}} = -\gamma_{\mathrm{LL}} \mathbf{M} \times \mathbf{H} - \frac{\gamma_{\mathrm{LL}} \alpha}{M_s} \mathbf{M} \times \mathbf{M} \times \mathbf{H}$ (see the Appendix for more details). Equation (3) is employed in the present study with an internal field combining the contributions from the Zeeman, magnetocrystalline, magnetodipolar, and exchange energies. The latter also includes a contribution from the phenomenological field that accounts for the exchange energy arising from changes of the magnetization vector length,[11,22,26–28] i.e., the exchange energy that is stored in thermal magnons, and cannot be explicitly accounted for on the micromagnetic scale. This field pushes the magnetization vector length back to its equilibrium value at the given temperature.

The simulations were carried out on a thin magnetic disk and an ellipse with a thickness of 7 nm. The diameter of the disk is 110 nm, while the ellipse has minor and major axes of 44 and 110 nm, respectively. The magnetic parameters are close to that of cobalt, i.e., a saturation magnetization of $M_s = 1440 \times 10^3$ A/m, exchange stiffness constant of $A_{ex} = 2.1 \times 10^{-11}$ J/m, and uniaxial anisotropy strength of $|K_u| = 5.2 \times 10^5$ J/m^3 (varied in some of the simulations). Cobalt has a hexagonal lattice for which the relaxation tensor is diagonal $\hat{\alpha} = \alpha \hat{\nu}$,[11,22] where $\hat{\nu}$ is a diagonal tensor which characterizes the relative degree of anisotropic damping. Cobalt is also characterized by a relatively strong magnetocrystalline anisotropy, making it an ideal candidate for our case study and for possible experiments. The damping constant α is fixed to 0.008 for both LLBar and LL, while the components of the tensor ν_{ii} are varied to mimic given crystallographic configurations. In the present study,we only focus on the saturated case to depict the main features of the anisotropic damping. For this purpose in all simulations we saturate the sample in-plane by using a sufficiently large applied magnetic field of 1 T.

The magnonic spectra are extracted by means of the FFT from 40-ns-long time traces of the net magnetization, simulated by exposing the relaxed magnetic states to a spatially uniform "sinc" excitation[29] with an amplitude of 0.01 T and cutoff frequency of 80 GHz. The bandwidth of the simulations is maintained at 100 GHz (Nyquist frequency) to avoid FFT aliasing. The magnetization dynamics always vanish within the time frame of the simulation. So we would not expect any artificial broadening of the magnonic resonances. Nevertheless, a windowing function is also applied before the FFT to prevent spectral leakage.

The dominant peaks in the spectra (attributed to the magnonic resonances of different spatial characters) are fitted to Lorentzian curves in order to extract their amplitudes, frequencies ω, and full width at half maximum $\triangle\omega$. The latter two parameters are used to estimate the relative net relaxation rates given by the Landau-Lifshitz-Baryakhtar and Landau-Lifshitz models as $\Gamma_{\mathrm{LLBar}} = \triangle\omega_{\mathrm{LLBar}}/\omega_{\mathrm{LLBar}}$ and $\Gamma_{\mathrm{LL}} = \triangle\omega_{\mathrm{LL}}/\omega_{\mathrm{LL}}$, respectively. Finally, the ratio between the two is calculated as $\eta = \Gamma_{\mathrm{LLBar}}/\Gamma_{\mathrm{LL}}$ to estimate the difference between the two micromagnetic models.

The spatial profiles of the magnonic modes are calculated using the method from Ref. 30. The typical spectra and spatial profiles of the modes are shown in Fig. 1. For the disk, we excite two dominant modes, one of "edge" (lowest magnonic mode) and one of "bulk" (higher-order magnonic mode) character for any direction of saturation (within $[0,\pi/2]$). In contrast, for an ellipse only the edge mode remains within the frequency bandwidth of the simulations for all saturation directions. When the ellipse is magnetized along the minor axis the bulk mode is shifted above 80 GHz due to the enhanced

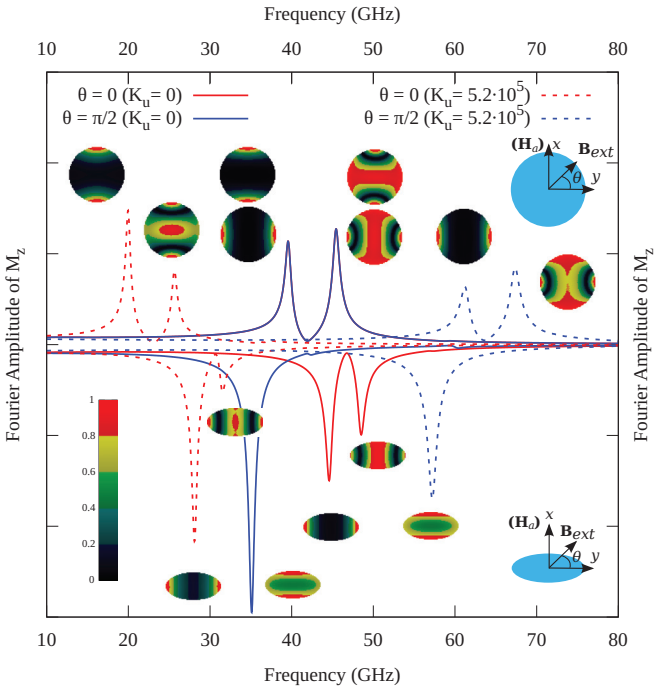

FIG. 1. (Color online) Spectra of the magnonic resonances and the corresponding spatial mode profiles are shown for a disk (top panel) and an ellipse (bottom panel). The solid and dashed lines correspond to isotropic and uniaxial materials, respectively.

contribution of exchange energy. The uniaxial anisotropy acts as expected from trivial physical considerations,[31] i.e., is hardening (softening) the magnonic resonances for the parallel (perpendicular) configurations.

In this work we consider nonconservative magnetization dynamics, i.e., the total angular momentum of the system is not conserved. However, the anisotropy axis represents a symmetry direction of the magnetic single crystal. Therefore projection of the total angular momentum on this axis should be conserved and there should be no relaxation of the magnetic moment along this axis. So the corresponding component of the relaxation tensor should be zero. However, real magnetic samples are typically polycrystalline and contain lattice defects, leading to scattering of magnons along the (effective) direction of crystallographic symmetry. So hereafter, we assume that the anisotropy of the damping is given by an order of magnitude reduction of the component along the symmetry axis.

Baryakhtar showed that components of the relaxation tensor can be expressed in terms of powers of magnetocrystalline anisotropy constants.[22] However, where the anisotropy constant is varied, the corresponding components of the damping tensor are kept constant to draw a straight comparison between LL and LLBar models. A more rigorous treatment, where relations between the components of the relaxation tensor and magnetocrystalline anistoropy constants are taken into account, is expected to change our results quantitatively, but not qualitatively.

The angular dependence of η calculated for the edge mode is shown in Fig. 2 for an isotropic Co disk (left panel) and an ellipse (right panel). For the disk the symmetry of η is either isotropic or twofold for an out-of-plane and in-plane reduction of the relaxation tensor, respectively. In contrast, for the ellipse the symmetry is always twofold, even for the case when the tensor is altered out of plane and, thereby, homogeneous in plane. So, surprisingly, the shape anisotropy also contributes to the symmetry of the relative relaxation rate. This is also supported by the fact that the relative relaxation rates are different for in-plane and out-of-plane reductions of the relaxation tensor, i.e., along easy and hard axes, respectively. Finally, the data suggest that changes of the relaxation constant along the saturation direction do not significantly change the value of the relative relaxation rate with respect to the one obtained from LL, i.e., $\eta \approx 1$.

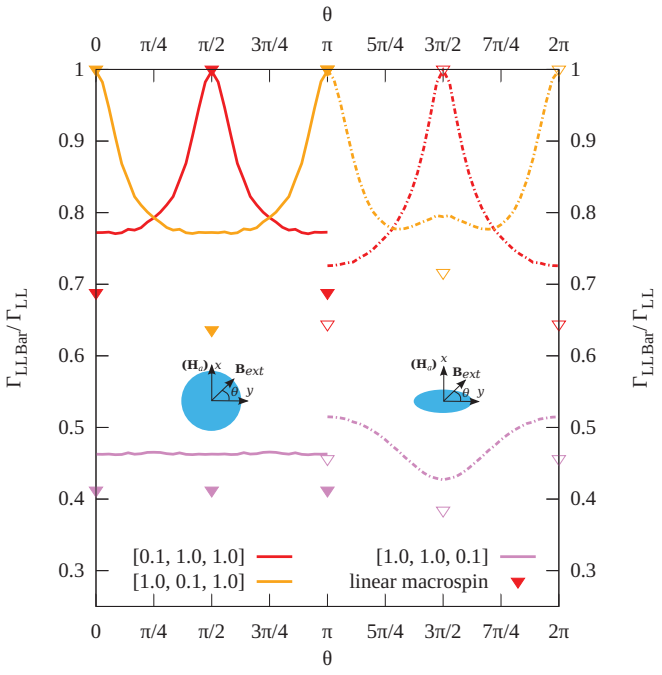

FIG. 2. (Color online) The angular dependence of the ratio between the relative relaxation rates of LLBar and LL is shown for different structures of the diagonal tensor $\hat{\nu}$. The ratio is extracted for the edge mode in an isotropic Co nanoelement ($|K_u| = 0$ J m^{-3}). The left $(0,\pi)$ and right $(\pi,2\pi)$ semiplanes correspond to the disk and an ellipse, respectively.

To interpret our observations, we would like to remind that the magnetization vector has three degrees of freedom. Two of them correspond to precession (transverse degrees of freedom) and one corresponds to the changes of the vector's length (longitudinal degree of freedom). These degrees of freedom also represent the relaxation channels for the magnons in magnetic systems. Since the relative relaxation rates calculated with LLBar and LL are found to be the same when samples are saturated along shortest eigenvector of the relaxation tensor, then one can conclude that in our particular case the longitudinal degree of freedom is not excited. Linearization of the LLBar equation in the macrospin approximation under assumption of diagonal relaxation tensor and constant magnetization length leads to (hereafter the Einstein summation convention is used)

$$\Gamma = \frac{1}{N}\alpha\nu_{ii}\frac{\omega_i}{\omega} \overset{N=2}{=} \frac{1}{2}\alpha(\epsilon\nu_{ii} + \epsilon^{-1}\nu_{jj}). \tag{4}$$

The frequency of the precession and ratio between characteristic frequencies are given by $\omega^2 = \omega_i\omega_j$ and $\epsilon = \sqrt{\omega_i/\omega_j}$, respectively $(i \neq j)$. N, ω_i, and ω_j denote the number of transverse degrees of freedom (that is 2 in our case) and their characteristic frequencies, respectively. Hereafter we refer to Eq. (4) as the linear macrospin model. It has a clear physical meaning, so that the amount of dissipated energy is the weighted sum of the energies stored in all degrees of freedom with weighting coefficients (which are given by the corresponding components of the relaxation tensor) that describe the symmetry and strength of the energy scattering from spins to the other subsystems. So the striking reduction of the relaxation rate with the out-of-plane component of the relaxation tensor suggests that for the given magnonic mode the out-of-plane degree of freedom stores more energy than the in-plane one. By estimating the ratio between the relative relaxation rates Γ/Γ' for two different structures of the tensor ν and ν', it is possible to find the characteristic frequencies of all degrees of freedom. In particular, for the out-of-plane component it reads

$$\omega_z = \sqrt{\frac{\nu_{ii} - (\Gamma/\Gamma')\nu'_{ii}}{(\Gamma/\Gamma')\nu'_{zz} - \nu_{zz}}}\omega, \quad i = x,y. \tag{5}$$

If the linear macrospin model is valid, then for the disk the frequency should be independent of the direction of in-plane saturation. For the lowest magnonic mode, the simulated relaxation rates for $\nu_{ii} = [0.1,1,1]$ and $\nu'_{ii} = [1,1,0.1]$ lead to the values of ω_z of ≈54.26 GHz and ≈47.94 GHz, at 0 rad

and $\frac{\pi}{2}$ rad, respectively. For the higher-order magnonic mode, the values of ω_z at 0 rad and $\frac{\pi}{2}$ rad are ≈62.54 GHz and ≈55.54 GHz, respectively.

The relative difference of $\frac{\omega_z(0)-\omega_z(\pi/2)}{\omega_z(0)} \approx 11.2\%$ between the values of ω_z at 0 and $\frac{\pi}{2}$ rad is roughly the same for these two modes, suggesting the presence of a damping mechanism beyond the trivial linear macrospin model. This angular dependency cannot be simply attributed to the artificial edge roughness (and corresponding two-magnon scattering relaxation mechanism), because bulk modes are not sensitive to it.[32] So we assume that the observed discrepancy is due to the nonlinear effects, i.e., excitation of the second harmonics. According to the simulations, the ratios between the amplitudes of the second harmonics and corresponding eigenmodes are around 10^{-3}. This dissipation channel is not accounted for in the linear macrospin model given by Eq. (4).

The analysis revealed the expected property of the shape anisotropy, i.e., that for the edge and bulk modes of the disk, the out-of-plane characteristic frequencies are much larger than the in-plane ones, $\omega_z \gg \omega_y$. However, the ratio between the characteristic frequencies might change for the higher-order modes because of interplay of the shape anisotropy and exchange energy as explained in Ref. 33. In particular, in thin magnetic nanoelements $\omega_y/\omega_z \ll 1$ and $\omega_y/\omega_z \to 1$ for low- and high-frequency magnons, respectively. Therefore we can expect that the relative relaxation rate is mode specific. The effect can only be accessed with full micromagnetic treatment, since the macrospin approximation cannot describe the nonzero-order magnons.

The frequency dependence of the relative relaxation rate, Γ_{LLBar}, of an isotropic disk with $\nu_{ii} = [0.1,1,1]$ is presented in Fig. 3. The striking feature here is the frequency dependence even when the relaxation tensor is effectively isotropic ($\theta = \pi/2$). This effect has been recently demonstrated experimentally by Nembach *et al.*[34] The relative linewidth decreases with the frequency of the mode, since in the exchange dominated regime the in-plane and out-of-plane characteristic frequencies converge to the same point, thereby equalizing both relaxation channels. So according to Eq. (4) for the exchange dominated magnons the relaxation rate eventually approaches the bottom limit defined by the components of the relaxation tensor, i.e., 0.0044 and 0.008 for $\theta = 0$ and $\theta = \pi/2$, respectively. The calculated values of the relaxation rate are higher than the intrinsic values fixed by the relaxation tensor, i.e., 0.013 and 0.023 for $\theta = 0$ and $\theta = \pi/2$, respectively. This can be attributed to the nonuniform spatial character of the magnonic modes.[35]

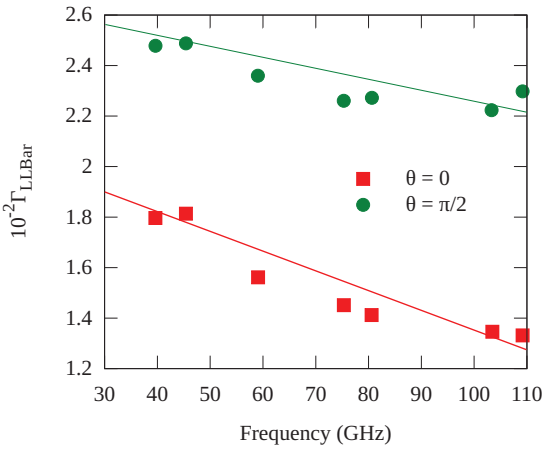

FIG. 3. (Color online) The frequency dependence of the relative relaxation rate in an isotropic Co disk ($|K_u| = 0$ J m^{-3}) is shown. The frequencies correspond to the eigenmodes of the disk. The straight lines are there to guide the eye. The diagonal components of the tensor $\hat{\nu}$ are [0.1,1,1]. $\theta = 0$ and $\theta = \pi/2$ correspond to anisotropic and effectively isotropic relaxation tensor, respectively.

Let us employ the linear macrospin model to explain the results obtained in an ellipse, which naturally introduces an in-plane shape anisotropy. For the cases of $\nu_{ii} = [0.1,1,1]$ at 0 rad (along the minor axis) and $\nu_{ii} = [1,0.1,1]$ at $\frac{\pi}{2}$ rad (along the major axis) the in-plane and out-of-plane characteristic frequencies are $\omega_x \approx 36.14$ GHz, $\omega_z \approx 55.11$ GHz and $\omega_y \approx 23.81$ GHz, $\omega_z \approx 51.11$ GHz, respectively. For both cases the ω_z is similar to that of the disk, while the in-plane characteristic frequency is enhanced (reduced) for saturation along the major (minor) due to the in-plane shape anisotropy.[36] For the quantity represented in Fig. 2 we can simply write

$$\eta = \frac{\Gamma_{\mathrm{LLBar}}}{\Gamma_{\mathrm{LL}}} = \frac{1}{1+\epsilon^{-2}}\nu_{ii} + \frac{1}{1+\epsilon^{2}}\nu_{jj}, \tag{6}$$

where $i = x,y$ for 0 and $\frac{\pi}{2}$ rad, respectively. These theoretical values are represented by dots in Fig. 2 and qualitatively mimic the behavior observed in Fig. 2.

In contrast to shape, magnetocrystalline anisotropy could be relatively easily tuned dynamically, i.e., in multiferroic materials.[37] The relative linewidth calculated on the same samples but in the presence of uniaxial anisotropy is shown in Fig. 4. The direction of uniaxial anisotropy always coincides with the shortest eigenvector of the damping tensor for the reasons explained above. The results presented in Fig. 4 qualitatively reproduce those from Fig. 2. For all the cases at 0 ($\frac{\pi}{2}$) rad the uniaxial anisotropy softens (hardens) the lowest magnonic mode thus reducing (enhancing) the influence of the in-plane relaxation channel. Therefore the relative relaxation rate is always enhanced as compared to the isotropic case. Furthermore, in the case of an ellipse for $\nu_{ii} = [1,0.1,1]$ at $\frac{\pi}{2}$ rad, the relative linewidth tends to unity. This effect could be easily explained if we take into account that shape and uniaxial anisotropies act in the same way, i.e., soften the lowest magnonic mode, eventually vanishing the role of in-plane relaxation. Since the out-of-plane relaxation channel is equivalent to that of the isotropic case, the linewidth tends to the one calculated with the LL equation.

So, by tuning the strength of the uniaxial anisotropy we can effectively change the relative relaxation rate within the limits defined by the anisotropy of the damping tensor. The relative linewidth as a function of the uniaxial anisotropy constant $|K_u|$ is shown in Fig. 5. A fit to the linear macrospin model is also shown. We assumed that the frequency of the mode is given by (SI units)

$$\omega = \omega_0 - \frac{(\gamma_{\mathrm{LL}}/2\pi)}{\mu_0 M_s}|K_u|, \tag{7}$$

where ω_0 is the frequency of the mode in the isotropic case with the assumption that contribution of the magnetocrystalline anisotropy is second order with respect to ω_0. So the ratio

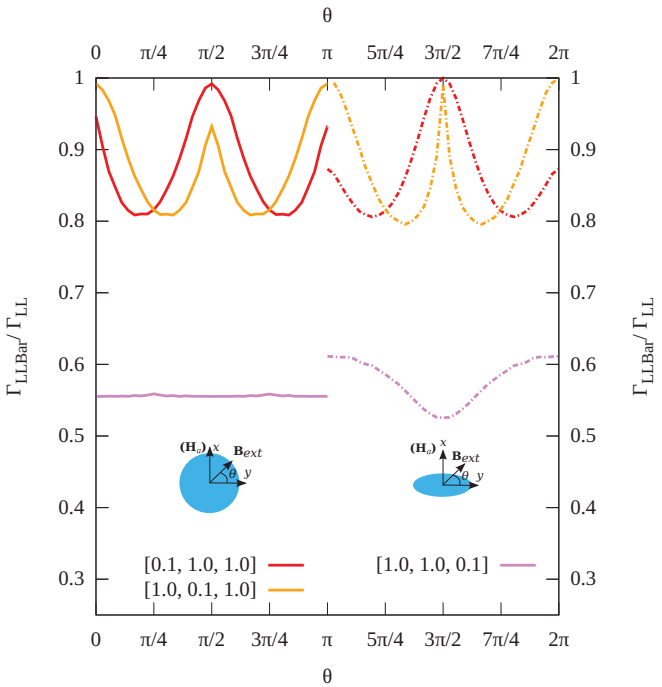

FIG. 4. (Color online) The angular dependence of the ratio between relative relaxation rates of LLBar and LL is shown for different structures of the tensor $\hat{\nu}$. The ratio is extracted for the edge mode in a uniaxial Co nanoelement ($|K_u| = 5.2 \times 10^5$ J m^{-3}). The left $(0,\pi)$ and right $(\pi,2\pi)$ semiplanes correspond to the disk and an ellipse, respectively.

of relative relaxation rates is given by

$$\eta = \frac{1}{1+(\omega_j/\omega)^2}\nu_{ii} + \frac{1}{1+(\omega/\omega_j)^2}\nu_{jj}, \quad i \neq j. \tag{8}$$

So by changing the strength of the magnetocrystalline anisotropy, we change the ellipse of motion, and thereby the relative contribution of the different relaxation channels. By aligning the easy axis with the shortest eigenvector of the relaxation tensor the anisotropy of the damping could be suppressed, i.e., $\eta \to 1$ when $K_u \to \frac{\mu_0 M_s \omega_0}{\gamma_{LL}/2\pi}$. The slight difference between the slopes of the curves calculated for the edge and bulk modes is due to the difference in ratio of characteristic frequencies ϵ of these two modes calculated with Eq. (6).

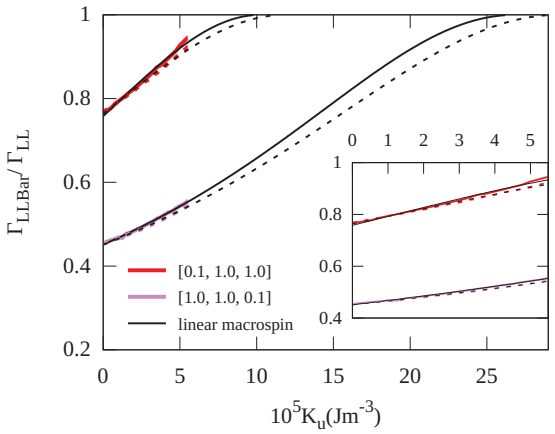

FIG. 5. (Color online) The ratio between the relative relaxation rates $\Gamma_{\mathrm{LLBar}}/\Gamma_{\mathrm{LL}}$ in function of the uniaxial anisotropy constant $|K_u|$ is shown for different structures of the tensor $\hat{\nu}$. The solid and dotted lines correspond to the "edge" and "bulk" modes of a uniaxial Co disk, respectively.

Based on our model and results obtained in an isotropic disk and an ellipse we conclude that (a) the highest reduction of relative relaxation rate is observed when the shortest eigenvector of the relaxation tensor is parallel to the hardest degree of freedom and (b) the reduction (enhancement) of characteristic frequency leads to the reduction (enhancement) of the contribution of corresponding relaxation channel. These conclusions could be used to design a representative experiment, e.g., measurements of the magnonic linewidths in Co nanoelements with in-plane and out-of-plane uniaxial anisotropies. Then by estimating the characteristic frequencies from the micromagnetic simulations, the corresponding components of the relaxation tensor could be extracted.

In conclusion, we showed that the symmetry of the magnonic relative relaxation rate with respect to the direction of saturation is determined by the superposition of the symmetries of the relaxation tensor and the ellipse of motion. The latter is mode-specific due to the competition between the shape anisotropy and the exchange energy (that eventually becomes dominant for high-order magnons), thereby making the absolute value of the relative relaxation rate frequency dependent. Moreover, it could be altered by changing the strength of the magnetocrystalline anisotropy, e.g., in multiferroic materials. Finally, our numerical implementation is open, and so, it can be freely used by the community to fit experimental data.

We would like to thank J. Leliaert for critical reading of the manuscript. A.V. acknowledges financial support from the Flanders Research Foundation (FWO).

APPENDIX

Here we would like to show how the LLBar reduces to the LL in the limiting case of the isotropic relaxation and conservative magnetization dynamics. So we start from the general Baryakhtar equation without the nonlocal damping term:

$$\frac{\partial \mathbf{M}}{\partial t} = -\gamma_{LL}\mathbf{M}\times\mathbf{H} + \hat{\lambda}(\mathbf{M})\mathbf{H}. \tag{A1}$$

Then we expand the damping tensor around the absolutely symmetric magnetic ground state as it was discussed above:

$$\hat{\lambda}(\mathbf{M}) = \hat{\lambda}(0) + \hat{\mu}_{pq}(0)M_p M_q + \cdots. \tag{A2}$$

Since the nonconservative zero-order term dominates in ferromagnetic metals, then

$$\hat{\lambda}(\mathbf{M}) \approx \hat{\lambda}(0) = -\gamma_{LL} M_s \hat{\alpha}, \tag{A3}$$

where $\hat{\alpha}$ is the dimensionless relaxation tensor. By representing $\mathbf{M}$ as $\mathbf{M} = M\mathbf{m}$, $\mathbf{m}$ is the unit vector, and substituting Eq. (A3) into Eq. (A1) we get

$$\frac{\partial M}{\partial t}\mathbf{m} + M\frac{\partial \mathbf{m}}{\partial t} = -\gamma_{LL} M\mathbf{m}\times\mathbf{H} - \gamma_{LL} M_s \hat{\alpha}\mathbf{H}. \tag{A4}$$

Now multiply Eq. (A4) by $\mathbf{m}$,

$$\frac{\partial M}{\partial t}\mathbf{m}^2 + \frac{1}{2}M\frac{\partial \mathbf{m}^2}{\partial t} = -\gamma_{LL}M\mathbf{m}[\mathbf{m}\times\mathbf{H}] - \gamma_{LL}M_s\mathbf{m}\hat{\alpha}\mathbf{H}. \tag{A5}$$

Taking into account that $\mathbf{m}^2 \equiv 1$, $\frac{\partial \mathbf{m}^2}{\partial t} \equiv 0$ and $\mathbf{m}[\mathbf{m}\times\mathbf{H}] \equiv 0$, Eq. (A5) reduces to

$$\frac{\partial M}{\partial t} = \gamma_{LL}M_s\mathbf{m}\hat{\alpha}\mathbf{H}. \tag{A6}$$

Then we substitute Eq. (A6) into Eq. (A4) and divide everything by M, so Eq. (A4) transforms into

$$\frac{\gamma_{LL}M_s}{M}\mathbf{m}\hat{\alpha}\mathbf{H}\mathbf{m} + \frac{\partial \mathbf{m}}{\partial t} = -\gamma_{LL}\mathbf{m}\times\mathbf{H} - \frac{\gamma_{LL}M_s}{M}\hat{\alpha}\mathbf{H}. \tag{A7}$$

By taking into account triple cross product property, i.e., $\mathbf{a}\times\mathbf{b}\times\mathbf{c} = \mathbf{b}(\mathbf{ac}) - \mathbf{c}(\mathbf{ab})$, we reduce Eq. (A7) to

$$\frac{\partial \mathbf{m}}{\partial t} = -\gamma_{LL}\mathbf{m}\times\mathbf{H} - \frac{\gamma_{LL}M_s}{M}\mathbf{m}\times\hat{\alpha}(\mathbf{m}\times\mathbf{H}). \tag{A8}$$

So Eqs. (A6) and (A8) form a system of coupled equations. However, if we assume that $\frac{\partial \mathbf{M}}{\partial t} \equiv 0$ (such as in LL model), then $M \equiv M_s$ and the system of equations given by Eqs. (A6) and (A8) reduces to a single equation,

$$\frac{\partial \mathbf{m}}{\partial t} = -\gamma_{LL}\mathbf{m}\times\mathbf{H} - \gamma_{LL}\mathbf{m}\times\hat{\alpha}(\mathbf{m}\times\mathbf{H}), \tag{A9}$$

that under assumption of isotropic damping tensor transforms to

$$\frac{\partial \mathbf{m}}{\partial t} = -\gamma_{LL}\mathbf{m}\times\mathbf{H} - \gamma_{LL}\alpha\mathbf{m}\times\mathbf{m}\times\mathbf{H}, \tag{A10}$$

which is the Landau-Lifshitz equation. The fact that in the limiting case LLBar reduces to LL shows self-consistency of the former. So if the magnetization dynamics is conservative, then nonconservative relaxation automatically transforms into conservative damping of the simplest LL form. Physically it means that in magnetic metals, the spin-electron scattering is not only responsible for the relaxation of the magnetization length, but also for the relaxation of precessional degrees of freedom.

*mykola.dvornik@ugent.be; http://dynamat.ugent.be

[1] L. D. Landau and E. Lifshitz, Phys. Z. Sowjet. **8**, 153 (1935).
[2] T. Gilbert, Phys. Rev. **100**, 1243 (1955).
[3] T. Gilbert, IEEE Trans. Magn. **40**, 3443 (2004).
[4] R. Kikuchi, J. Appl. Phys. **27**, 1352 (1956).
[5] H. Yu, R. Huber, T. Schwarze, F. Brandl, T. Rapp, P. Berberich, G. Duerr, and D. Grundler, Appl. Phys. Lett. **100**, 262412 (2012).
[6] X. Joyeux, T. Devolder, J. V. Kim, Y. G. de la Torre, S. Eimer, and C. Chappert, J. Appl. Phys. **110**, 063915 (2011).
[7] V. V. Kruglyak, S. O. Demokritov, and D. Grundler, J. Phys. D: Appl. Phys. **43**, 260301 (2010).
[8] K. Gilmore, Y. U. Idzerda, and M. D. Stiles, Phys. Rev. Lett. **99**, 027204 (2007).
[9] V. Tiberkevich and A. Slavin, Phys. Rev. B **75**, 014440 (2007).
[10] M. Fahnle, D. Steiauf, and C. Illg, Phys. Rev. B **84**, 172403 (2011).
[11] I. V. Baryakhtar and V. G. Baryakhtar, Ukr. J. Phys. **43**, 1433 (1998).
[12] V. Heine, Phys. Rev. **153**, 673 (1967).
[13] P. S. Keatley, P. Gangmei, M. Dvornik, R. J. Hicken, J. R. Childress, and J. A. Katine, Appl. Phys. Lett. **98**, 082506 (2011).
[14] S. Serrano-Guisan, K. Rott, G. Reiss, and H. W. Schumacher, J. Phys. D: Appl. Phys. **41**, 164015 (2008).
[15] H. W. Schumacher, S. Serrano-Guisan, K. Rott, and G. Reiss, Appl. Phys. Lett. **90**, 042504 (2007).
[16] S. Mizukami, Y. Ando, and T. Miyazaki, Jpn. J. Appl. Phys. **40**, 580 (2000).
[17] M. L. Schneider, J. M. Shaw, A. B. Kos, T. Gerrits, T. J. Silva, and R. D. McMichael, J. Appl. Phys. **102**, 103909 (2007).
[18] M. Buchmeier, D. E. Bürgler, P. A. Grünberg, C. M. Schneider, R. Meijers, R. Calarco, C. Raeder, and M. Farle, Phys. Status Solidi A **203**, 1567 (2006).
[19] A. Vansteenkiste and B. Van de Wiele, J. Magn. Magn. Mater. **323**, 2585 (2011).
[20] M. Fähnle and S. Zhang, J. Magn. Magn. Mater. **326**, 232 (2013).
[21] W. Wang, M. Dvornik, M.-A. Bisotti, D. Chernyshenko, M. Beg, M. Albert, A. Vansteenkiste, B. Van Waeyenberge, V. V. Kruglyak, and H. Fangohr (unpublished).
[22] V. G. Bar'yakhtar and A. G. Danilevich, Low Temp. Phys. **36**, 303 (2010).
[23] J. H. Mentink, J. Hellsvik, D. V. Afanasiev, B. A. Ivanov, A. Kirilyuk, A. V. Kimel, O. Eriksson, M. I. Katsnelson, and T. Rasing, Phys. Rev. Lett. **108**, 057202 (2012).
[24] B. Koopmans, G. Malinowski, F. Dalla Longa, D. Steiauf, M. Fahnle, T. Roth, M. Cinchetti, and M. Aeschlimann, Nat. Mater. **9**, 259 (2010).
[25] T. Roth, A. J. Schellekens, S. Alebrand, O. Schmitt, D. Steil, B. Koopmans, M. Cinchetti, and M. Aeschlimann, Phys. Rev. X **2**, 021006 (2012).
[26] U. Atxitia, O. Chubykalo-Fesenko, J. Walowski, A. Mann, and M. Münzenberg, Phys. Rev. B **81**, 174401 (2010).
[27] U. Atxitia and O. Chubykalo-Fesenko, Phys. Rev. B **84**, 144414 (2011).
[28] R. F. L. Evans, D. Hinzke, U. Atxitia, U. Nowak, R. W. Chantrell, and O. Chubykalo-Fesenko, Phys. Rev. B **85**, 014433 (2012).
[29] M. Dvornik, A. N. Kuchko, and V. V. Kruglyak, J. Appl. Phys. **109**, 07D350 (2011).
[30] M. Dvornik, P. V. Bondarenko, B. A. Ivanov, and V. V. Kruglyak, J. Appl. Phys. **109**, 07B912 (2011).
[31] A. G. Gurevich and G. A. Melkov, *Magnetization Oscillations and Waves* (CRC Press, Boca Raton, FL, 1996).
[32] B. B. Maranville, R. D. McMichael, S. A. Kim, W. L. Johnson, C. A. Ross, and J. Y. Cheng, J. Appl. Phys. **99**, 08C703 (2006).
[33] M. Dvornik and V. V. Kruglyak, Phys. Rev. B **84**, 140405 (2011).
[34] H. T. Nembach, J. M. Shaw, C. T. Boone, and T. J. Silva, Phys. Rev. Lett. **110**, 117201 (2013).
[35] B. Hillebrands and K. Ounadjela, *Topics in Applied Physics* (Springer, Berlin, 2002), p. 23.
[36] M. Pardavi-Horvath, B. G. Ng, F. J. Castano, H. S. Körner, C. Garcia, and C. A. Ross, J. Appl. Phys. **110**, 053921 (2011).
[37] Y. Wang, J. Hu, Y. Lin, and C.-W. Nan, NPG Asia Mater. **2**, 61 (2010).